LAWRENCE
LIVERMORE
NATIONAL
LABORATORY

LLNL-JRNL-410054

The Origin of Refractory Minerals in Comet 81P/Wild 2

M. Chi, H. A. Ishii, S. B. Simon, J. P. Bradley, Z. R. Dai, D. J. Joswiak, N. D. Browning, G. Matrajt

January 23, 2009

Geochimica et Cosmochimica Acta

Disclaimer

The origin of refractory minerals in Comet 81P/Wild 2

Miaofang Chi[a,b], Hope A. Ishii[a,]*, Steven B. Simon[c], John P. Bradley[a], Zurong Dai[a], David Joswiak[d], Nigel D. Browning[b] and Graciela Matrajt[d]

[a] Institute of Geophysics and Planetary Physics, Lawrence Livermore National Laboratory, Livermore, CA 94550 USA

[b] Department of Chemical Engineering and Materials Science, University of California at Davis, Davis, CA 95616 USA

[c] Department of the Geophysical Sciences, 5734 S. Ellis Ave., The University of Chicago, Chicago, IL 60637, USA

[d] Department of Astronomy, University of Washington, Seattle WA 98195, USA

* Corresponding author.

E-mail address: hope.ishii@llnl.gov (H. A. Ishii).

To be submitted to *Geochimica et Cosmochimica Acta*

Abstract

Refractory Ti-bearing minerals in the calcium-, aluminium-rich inclusion (CAI) Inti, recovered from the comet 81P/Wild 2 sample, were examined using analytical (scanning) transmission electron microscopy (STEM) methods including imaging, nanodiffraction, energy dispersive spectroscopy (EDX) and electron energy loss spectroscopy (EELS). Inti fassaite ($Ca(Mg,Ti,Al)(Si,Al)_2O_6$) was found to have a Ti^{3+}/Ti^{4+} ratio of 2.0±0.2, consistent with fassaite in other solar system CAIs. The oxygen fugacity ($\log f_{O_2}$) of formation estimated from this ratio, assuming equilibration among phases at 1509K, is -19.4±1.3. This value is near the canonical solar nebula value (-18.1±0.3) and in close agreement with that reported for fassaite-bearing Allende CAIs (-19.8±0.9) by other researchers using the same assumptions. Nanocrystals of osbornite (Ti(V)N), 2-40 nm in diameter, are embedded as inclusions within anorthite, spinel and diopside in Inti. Vanadium is heterogeneously distributed within some osbornite crystals. Compositions range from pure TiN to $Ti_{0.36}V_{0.64}N$. The possible presence of oxide and carbide in solid solution with the osbornite was evaluated. The osbornite may contain O but does not contain C. The presence of osbornite, likely a refractory early condensate, together with the other refractory minerals in Inti, indicates that the parent comet contains solids that condensed closer to the proto-sun than the distance at which the parent comet itself accreted. The estimated oxygen fugacity and the reported isotopic and chemical compositions are consistent with Inti originating in the inner solar system as opposed to it being a surviving CAI from an extrasolar source. These results provide insight for evaluating the validity of models of radial mass transport dynamics in the early solar system. The oxidation environments inferred for the Inti mineral assemblage are inconsistent

1 with an X-wind formation scenario. In contrast, radial mixing models allowing
2 accretion of components from different heliocentric distances can satisfy the
3 observations from the cometary CAI Inti.
4

1. INTRODUCTION

In January 2006 the NASA Stardust mission returned less than a milligram of solid sample from comet 81P/Wild 2. This is the first-ever sample return of material from a known body outside of the Earth-Moon system. Since comet 81P/Wild 2 is believed to have accreted beyond the giant planets, the returned samples were expected to be primitive, that is, rich in materials from the cold outer solar system, including abundant presolar grains inherited from the parent presolar molecular cloud. These primitive grains were expected to include some that formed in the outflows of other stars (i.e. true stardust) as well as grains that formed in the interstellar medium. The unexpected discovery within months of the sample's return of a calcium-, aluminium-rich inclusion (CAI), subsequently named "Inti", revealed that comet Wild 2 contains anhydrous, high-temperature phases similar to those found in chondritic meteorites from the asteroid belt (Brownlee et al., 2006; Zolensky et al., 2006). CAIs are believed to have formed 1-2 Myr after the initial collapse of the solar nebula and are among the earliest solids formed in the solar system (Hutchison et al., 2001). The Inti CAI has been found to contain Ti-rich pyroxene (often referred to as fassaite) ($Ca(Mg,Ti,Al)(Si,Al)_2O_6$), gehlenite ($Ca_2Al_2SiO_7$), perovskite ($CaTiO_3$), diopside $(Ca,Mg,Al)_2(Si,Al)_2O_6$), spinel ($MgAl_2O_4$) and anorthite ($CaAl_2Si_2O_8$), with osbornite (Ti(V)N) occuring as inclusions in silicates (Zolensky et al., 2006; Joswiak et al., 2008; Simon et al., 2008). Improved knowledge of the formation environment of these refractory minerals can provide a better understanding of how these minerals came to be incorporated into an outer solar system comet, 81P/Wild 2, and of the mechanisms of transport dynamics active during early solar system formation.

Two Ti-bearing refractory minerals in Inti, Ti-pyroxene (fassaite) and osbornite, are of special cosmochemical significance because they serve as potential recorders of the redox state of their formation environment. The oxidation states of transition metal elements in minerals are closely related to the oxygen fugacities of their formation environments (Stolper et al., 1982; Papike et al., 2005). In particular, the oxidation state of Ti in Ti-pyroxene in CAIs has been experimentally calibrated at one temperature (Beckett, 1986; Grossman et al., 2008) allowing it to serve as an oxygen barometer in CAIs for estimation of the oxygen fugacity at the time and place of their formation. The formation of osbornite occurs at higher temperatures than fassaitic pyroxene, possibly higher than 2000K depending on the local oxygen fugacity, total pressure and C/O ratio (Zolensky et al., 2006). Osbornite is stable in systems that are otherwise solar in composition for atomic C/O ratios between ~0.8 and 1 (~2 × solar), according to equilibrium thermodynamic calculations (Ebel, 2006).

In this work, we report the Ti oxidation states in Inti Ti-pyroxene (fassaite), compare the fassaite oxidation states from Inti with an Allende fassaite, and obtain a measure of the Ti^{3+}/Ti^{4+} ratio for Inti using oxidation state endmember oxides, $SrTiO_3$ and $LaTiO_3$. The Ti^{3+}/Ti^{4+} ratio obtained was then used to estimate the oxygen fugacity of the environment in which the Inti Ti-pyroxene formed by following calculation methods previously applied to fassaitic pyroxene found in refractory inclusions in the Allende meteorite. We also closely studied the Inti osbornite for evidence of coexistence of Ti-nitride, -oxide and -carbide as a means of potentially constraining the environment in which the osbornite formed. If TiO coexists with TiN, for example, the constraints in temperature and C/O ratio for the formation of 81P/Wild 2 osbornite are considerably narrowed relative to those for TiN alone (Ebel, 2006). Finally, we discuss the implications of these results with respect to the

formation environment(s) for Inti components and material transport in the early solar system.

2. TECHNIQUES

The 81P/Wild 2 dust sample was collected by hypervelocity impact at 6.1 km/s into aerogel (Brownlee et al., 2006). The impact track containing the Stardust CAI was initially harvested from a ~3 mm thick slab produced from an aerogel cell using an ultrasonic band saw. A ~200,000 rpm dental drill with a ~0.5 mm wide carbide burr was used to remove ~1 mm from each side of the slab at the University of Washington. Using the drill, the remaining slab was further reduced to a sliver of aerogel containing the impact track. The terminal particle, referred to as "Inti", was extracted and embedded in acrylic resin, and the remaining aerogel was pressed between Mylar films and then embedded in acrylic resin using the process of Matrajt and Brownlee (2006). Electron-transparent thin sections of the particles were produced using an ultramicrotome equipped with a diamond knife. Sections 50-80 nm thick were mounted on continuous-carbon substrates supported on 3 mm diameter Cu-mesh TEM grids. We studied three TEM specimens prepared from Inti.

Additional samples were prepared for comparisons with specific mineral components of the Inti CAI. For comparison with Inti fassaitic pyroxene, an electron probe microanalysis (EPMA) traverse was carried out on a large pyroxene crystal in a Type B2 CAI, TS65, from the Allende meteorite using the Cameca SX50 at the University of Chicago. Spot measurements were collected at 40 micron intervals. Ti oxidation states along the traverse were calculated by stoichiometry, and electron-transparent thin sections from three selected locations were prepared for TEM

analyses. These sections were prepared using an FEI Nova NanoLab 600 dual-beam focused ion beam (FIB) instrument in which a focused beam of 30 keV Ga+ ions is used to mill out sections and thin them to electron transparency for TEM analyses (e.g. Ishii et al., 2008). For additional comparisons with Inti fassaitic pyroxene, TEM specimens of end member oxides for Ti^{3+} and Ti^{4+}, $LaTiO_3$ and $SrTiO_3$ respectively, were prepared by the traditional preparation methods for electron-transparent sections: mechanical polishing followed by Ar ion milling. For comparison with Inti osbornite, TiN, TiO and TiC standard powders (99.5% (metals basis) from Alpha Aesar) were dispersed directly on holey carbon substrates on Cu TEM grids. Holey carbon substrates permitted the standards to be analysed without substrate interferences where the powder grains lie over an open hole. TiC powder was also dispersed on standard continuous-carbon substrates on Cu TEM grids.

(Scanning) transmission electron microscopy (STEM) combined with both energy dispersive x-ray spectroscopy (EDX) and electron energy loss spectroscopy (EELS) was used to investigate the compositions and crystal structures of the refractory minerals in Inti. The combination of these techniques provides simultaneous imaging and chemical analysis at high spatial resolution, capabilities that are necessary for characterizing the mineralogy of Inti because it is heterogeneous on a submicrometer scale. In this study, the chemical analyses were precisely correlated with local microstructures and petrography.

The microscope used in this work is an FEI Tecnai F20 G2 UT (S)TEM microscope equipped with a high angle annular dark field (HAADF) detector, an EDAX Genesis 4000 Si(Li) solid state energy-dispersive x-ray detector and a Gatan Imaging Filter (GIF) Tridiem high-resolution EELS spectrometer. All EELS spectra were recorded with a collection angle of 5.6 mrad and a dispersion of 0.1 eV/channel

with 2048 channels. The EELS energy resolution is 0.7 eV with 3 seconds acquisition time, and the spatial resolution is ~0.16 nm. The energy shift of each spectrum was calibrated by a reference zero-loss peak taken immediately after each core-loss edge spectrum.

The oxidation state of Ti in fassaitic pyroxene was investigated by EELS using the Ti-L edges. Although the Ti^{3+}/Ti^{4+} ratio can, in theory, be calculated by quantitative measurement of O and Ti using TEM-EDX, this approach is especially unreliable here because of the close petrographic association of the fassaite with other oxygen-rich silicate minerals and also with the silica aerogel capture medium. The oxygen signal is subject to further attenuation by light element x-ray absorption effects caused by specimen thickness. Ti oxidation state studies via Ti-L edge EELS, in contrast, are not subject to these complications. The L-edges of 3d-transition metal elements, with their sharp "white lines", are highly sensitive to the valence state of the element and thus have been widely used to investigate oxidation states in minerals and materials science studies (Leapman et al., 1982; Sparrow et al., 1984; Brydson et al., 1987; Colliex et al., 1991; Egerton, 1996; Zega et al., 2003; Garvie et al., 2004). The question of coexistence of TiN with TiO and TiC was addressed using high-resolution transmission electron microscopy (HRTEM), electron diffraction, energy filtered TEM (EFTEM), and electron energy loss spectroscopy (EELS).

3. RESULTS

Results of the TEM analyses, Ti valence measurements and exploration of the presence of O and C in the Inti osbornite are described below.

3.1 Minerals present in Inti

The following silicates and oxides have been identified in Inti (Zolensky et al., 2006) using electron diffraction and energy-dispersive x-ray spectroscopy: Ti-rich pyroxene (fassaite); gehlenitic melilite; perovskite; diopside; spinel; anorthite; and osbornite (nominally TiN). The chemistries and petrographic occurrences of these minerals have been described in some detail elsewhere (Zolensky et al., 2006; Simon et al., 2008), and we focus here on the Ti-bearing minerals fassaitic pyroxene and osbornite. Perovskite ($CaTiO_3$) is low in abundance in Inti and is absent from the three TEM specimens analyzed for this study. A typical STEM image of an Inti sample is shown in Figure 1. The circles mark the locations of osbornite inclusions. With the exception of the osbornite, the mineralogy and measured mineral compositions are similar to those in CAIs in meteorites. We have identified rounded and subhedral osbornite nanocrystals ranging in size from 2 to 40 nm in diameter and embedded as inclusions within anorthite, spinel and diopside. Most osbornite grains contain V distributed heterogeneously (see Figure 2), with V abundances varying from 0 to 64 atomic % (from TiN to $Ti_{0.36}V_{0.64}N$). Identifications were made by imaging (Figs. 1 & 2a), nanodiffraction (Fig. 2b) and EELS (Fig. 3) in the (S)TEM. Detailed discussion of the Ti-pyroxene and osbornite follow.

3.2 Valence state of Ti in Inti pyroxene

The compositions of several Inti Ti-rich fassaitic pyroxenes ($Ca(Mg,Ti,Al)(Si,Al)_2O_6$) were determined by TEM-EDX quantification analysis and are given in Table 1. Total TiO_2 contents vary between 3.7 and 14.5 weight %. We

investigated the valence states of Ti by collecting EELS at the Ti-L edges. Approximately 50 EELS spectra were collected from 6 Ti-pyroxene grains identified in the Inti samples. The spectra are essentially identical with consistent fine structure and energy shifts. A representative EELS spectrum from the Inti pyroxene is included in Figure 4a. The Ti-L edges in Inti fassaitic pyroxene were compared with those from a well-characterized meteoritic pyroxene and from synthetic $LaTiO_3$ (Ti^{3+} end member) and $SrTiO_3$ (Ti^{4+} end member) to obtain a measurement of the Ti^{3+}/Ti^{4+} ratio in the Inti pyroxene.

Ti-L edge EELS were collected from three TEM sections of fassaitic pyroxene prepared from a Type B CAI (TS65) from the Allende meteorite. These spectra were acquired under the same microscopy conditions as those for Stardust Inti samples, and they are compared with the Inti fassaitic pyroxene in Figure 4a. Ti^{3+}/Ti^{4+} ratios derived from electron probe microanalysis for the three meteoritic fassaitic pyroxene TEM specimens are 1.35±0.38, 2.15±1.07 and 1.48±0.84 for Positions 1, 2, and 3, respectively. These ratios are obtained by requiring stoichiometric oxides of all cations. The uncertainties do not reflect limitations of the EPMA analyses. Instead, they incorporate the combined effects of potential error in position from FIB specimen preparation and of local variation of Ti valency around the position from which each TEM specimen was extracted. Despite the capability to locate a particular feature with sub-micrometer precision in the FIB, there are large uncertainties in correlating the Ti^{3+}/Ti^{4+} ratios obtained from the electron microprobe analyses with those of the FIB-prepared TEM sections due to the uncertainty involved in extracting the TEM sections at the exact positions of the microprobe spot measurements (collected at 40 micrometer intervals rather than at specific features). The increased error in Ti valency for positions 2 and 3 is due to the rapid local variation of the Ti

valency around these positions as measured by EPMA. The different fine structures displayed at the three positions (Fig. 4a) indicate that the Ti^{3+}/Ti^{4+} ratio increases from Position 3 to Position 1 to Position 2. (The EPMA ratio given above for Position 3 is slightly greater than that for Position 1; however, they are within error of each other.) Careful comparison of the Ti-L edge fine structures between the Inti fassaitic pyroxene and the Allende fassaitic pyroxene shows that the fine structure of the Inti Ti L-edges, and therefore, the Ti oxidation state, is most similar to that of the Allende fassaitic pyroxene at Position 2, which has a Ti^{3+}/Ti^{4+} ratio of 2.15±1.07. Therefore, the dominant valance state of Ti in the Inti fassaitic pyroxene is 3+, and the Ti^{3+}/Ti^{4+} ratio falls in the range of 1.1-3.1 (or $Ti^{3+}/(Ti^{3+}+Ti^{4+}) \sim 0.52$-$0.75$), as do most analyses of fassaite from meteoritic CAIs (e.g., Simon and Grossman, 2006). The large range for the present results is due primarily to the large variation in the Ti oxidation state around Position 2 along the Allende fassaitic pyroxene EPMA line profile.

To improve the precision of the Ti^{3+}/Ti^{4+} ratio determination for the Inti fassaitic pyroxene, we modelled the Ti-L edges in the EEL spectra as a linear combination of the spectra of Ti^{3+} and Ti^{4+} in $LaTi^{3+}O_3$ and $SrTi^{4+}O_3$ respectively. Since the Ti ions in these oxides reside in TiO_6 octahedral sites, as do those in Ti-rich pyroxenes, comparing linear combinations of the Ti EELS from the oxide standards with the Inti pyroxene provides a better-constrained means of estimating the Inti Ti^{3+}/Ti^{4+} ratio. Figure 4b shows the Ti-L edge structures of the Inti Ti-pyroxene, the $LaTi^{3+}O_3$ and $SrTi^{4+}O_3$ standards, and a series of linear combinations of the spectra of the two oxide standards, given as $LaTiO_3$:$SrTiO_3$ ratios. By comparing Ti-L edges from the Inti fassaitic pyroxene and those from $LaTiO_3$ and $SrTiO_3$ in Figure 4b, it is evident that the peaks labelled A, B, C and D in the Inti fassaitic pyroxene spectrum are a result of combinations of Ti^{3+} (represented by $LaTiO_3$ with strong peaks at A and C) and Ti^{4+}

(represented by $LaTiO_3$ with strong peaks at B and D). Spectra "d" and "e" most closely resemble that of Inti fassaitic pyroxene. This indicates that the Ti^{3+}/Ti^{4+} ratio in the Inti fassaitic pyroxene falls in the range of 1.8-2.2 (or $Ti^{3+}/(Ti^{3+}+Ti^{4+}) \sim 0.64$-0.69). This result lies within the range determined above by comparison to Allende fassaitic pyroxene and the range reported by Simon and Grossman (2006). Therefore, both the comparison with Allende fassaitic pyroxene and the calculation of the contribution of Ti^{3+} and Ti^{4+} by linear combinations of endmember standards indicate a relatively high Ti^{3+}/Ti^{4+} ratio of approximately 2 in the Inti fassaitic pyroxene.

3.3 Solid solution of O and C in Inti osbornite?

Since the presence or absence of oxygen and/or carbon in solid solution in Inti osbornite would further constrain the osbornite formation conditions, we carried out studies to assess both possibilities. We investigated whether the osbornite in Inti contains O by combining several different TEM techniques, including energy filtered imaging and EELS spectroscopy. Detailed characterization of a typical osbornite particle is shown in Figure 2. As illustrated by the thickness map in Figure 2d, no abrupt thickness change is observable at the interface of the osbornite and its host, confirming that it is an embedded inclusion rather than a separate particle lying above or below the surface of the host. The host silicate and oxide matrices contain O, so the question of coexistence of oxide and nitride as a solid solution in the osbornite particle cannot be addressed by simply determining whether O is present at the osbornite location since O may be detected from the matrix surrounding the inclusion. High-resolution TEM imaging and nano-diffraction are also inconclusive: They show that the osbornite inclusions have the NaCl-type (rock salt) structure with a lattice

parameter of a_o~4.21Å (Figs. 2b & 2c). However, Ti(V)N and Ti(V)O both have the rock-salt structure with similar lattice parameters (a=4.185 Å for TiO and a=4.241 Å for TiN, JCPDS cards: No. 77-2170 & JCPDS card: No. 38-1420).

Energy filtered TEM (EFTEM) elemental maps of Inti osbornite inclusions were obtained using the 3-window method (Egerton, 1996). In this method, counts are integrated at each map pixel in three energy windows, two at energies below the absorption edge of the relevant element to establish the appropriate background to subtract from the third integrated window, which is set at an energy above the absorption edge. The intensity at each elemental map pixel is thus representative of the amount of that particular element present. These 3-window maps show that the Inti osbornite contains Ti, V and N (Figs. 2f-h). Similarly, a 3-window map could also indicate whether the osbornite, like the diopside host, contains O; however, the V absorption edges occur very near to the O edge, preventing an accurate establishment of the background for subtraction. An O post-edge image (with a window of 15 eV) is shown instead in Figure 2e. The post-edge image was obtained from a single energy window set above the O-K edge without any background subtraction. It is important to note that the V absorption edges produce additional background, larger with increasing V concentration, under the higher energy O edge so that the O post-edge image is expected to reflect the presence of V as well as O. A comparison of the O post-edge image in Figure 2e and the V EFTEM image in Figure 2g shows that they do not display the same intensity pattern. If the high intensity regions in the O post-edge image correlated with the high intensity regions in the V EFTEM image, then the higher intensity in the O post-edge image at the osbornite inclusion could be attributed entirely to V contributions to an increased background at the osbornite. Instead, the differing intensity patterns between the O post-edge image and the V

EFTEM image suggest that the inclusion likely contains some O. In principle, this suggestion might readily be confirmed by collecting EELS on and off the osbornite inclusion since solid solution of O in TiN results in fine structure changes on the O-K edge. However, due to the high background O signal from the surrounding silicate matrix, the signal from a small amount of O in solid solution in TiN cannot be distinguished with any certainty. The O-K and Ti-L edges are also significantly perturbed by V, which is present in varying concentrations in Inti osbornite, as can be seen in Figure 3 in the differing relative amplitudes of the V-L and Ti-L edges from three osbornite inclusions labelled "A", "B" and "C". Since inclusion "C" (Fig. 3) is almost V-free, as are meteoritic osbornites reported to date (Weisberg, 1988; Meibom et al., 2007), the slight shift of the Ti-L edges to lower energy and the fine structure changes of the N-K edge in the spectrum of inclusion "C", compared with those of the standard TiN, are most likely a result of O present in solid solution in this inclusion. Based on these results, we conclude that it is possible that some O is present in solid solution in the Ti(V)N inclusions in Inti. However, most of the inclusions contain V, so solid solution of O in all of the Inti osbornite cannot be claimed with any certainty.

Titanium carbide (TiC) is predicted to form with osbornite (TiN) by gas-solid condensation from a fractionated nebular gas with a high C/O ratio (0.96-0.97) (Petaev et al., 2001; Ebel, 2006). NanoSIMS measurements by Meibom and coworkers (2007) indicate that C is present in solid solution in osbornite in a refractory inclusion in the Isheyevo meteorite. However, we did not detect C in any of the Inti osbornite inclusions by EELS, and C in TiC should be easily distinguished by EELS from C in the supporting C film due to the significantly different fine structures of C-K edges in these bonding environments. The lack of C in the Inti osbornite is also evident based on our measurements on TiC standard particles of various sizes on

C film. These measurements show that the EELS feature of a TiC particle ~4 nm in diameter is still detectable on a carbon film with a thickness comparable to those supporting the Stardust specimens.

4. DISCUSSION

4.1 Comparison of Inti osbornite with meteoritic occurrences

The majority of minerals present in Inti are similar to those in CAIs in meteorites. The osbornite in Inti, however, differs even from those rare occurrences of meteoritic osbornite reported to date by Meibom et al. (2007) in a refractory inclusion in the Isheyevo CH/CB chondrite and by Weisberg et al. (1998) in the ALH85085 CH chondrite. The first difference is in grain size. Inti osbornite is present as inclusions tens of nanometers in diameter, whereas the meteoritic osbornite grains that have been identified are tens of micrometers in diameter. Inti osbornite also contains heterogeneously distributed V in some nanocrystals, with abundances ranging from 0 to 64 atomic %. Meibom et al. (2007) did not detect any transition metal other than Ti. In addition, they clearly identified C in the Isheyevo osbornite, whereas C is not present in the Inti osbornite grains studied in the present work. The osbornite petrographic associations are also not identical among these three cases. In ALH85085, osbornite is associated with spinel, whereas osbornite in Isheyevo is associated with spinel, melilite, grossite and aluminous diopside. The osbornite particles in Inti found to date are correlated with anorthite, spinel and diopside.

The variability of V content within single sub-micrometer-sized osbornite grains in Inti indicates a non-equilibrated state. The nitrides of both Ti and V

condense at higher temperatures than the respective metals (Enomoto, 1996), so the Ti(V)N osbornite grains in Inti almost certainly represent direct condensates from the local nebular gas. Experiments involving annealing of Ti/V multilayers in a conventional furnace with nitriding gases have shown that interdiffusion and homogenization of Ti and V nitride layers occur at temperatures near 1100K (Galesic et al., 2000) in terrestrial laboratory conditions. The relevant homogenization temperature under the conditions of formation for Inti osbornite is unknown. EELS studies on TiN/VN multilayers grown directly as nitrides also exhibit interdiffusion (Lazar et al., 2008). The Ti-V chemical gradients remaining within single osbornite grains may indicate that the grains cooled fairly rapidly after formation and never annealed at a temperature sufficient to produce homogenization. Possible implications of the V content variability are that the osbornite condensed under dynamic nebular conditions or that there were multiple growth and/or evaporation events in differing formation environments. In other words, the osbornite formation environment may have changed due to changing spatial location within the nebula during transport of the CAI particle, due to evolution of the local nebular conditions over a period of time, or due to both.

The inclusion of Inti osbornite particles within matrix hosts indicates that they must have formed prior to, or with, their hosts, namely anorthite, spinel and diopside. It is interesting to note that osbornite has yet to be identified embedded in Ti-rich pyroxene (fassaite). If it continues to hold true in future studies of Inti samples, this is an important observation: In that case, the formation environment constraints established for the Inti fassaitic pyroxene and the Inti osbornite are not mutually constraining. These issues are discussed in more detail below.

4.2 Estimate of oxygen fugacity from Inti fassaitic pyroxene

Studies show that the predominant valence of Ti in pyroxenes is 4+ at $\log f_{O_2}$ above ~ IW-7 (7 orders of magnitude lower than the iron–wüstite (IW) oxygen buffer) (Papike et al., 2005). The high Ti^{3+}/Ti^{4+} ratio (2.0±0.2) in Inti fassaitic pyroxene thus suggests that it condensed in a highly reducing atmosphere. This ratio, in combination with the local mineral chemistry, can be used to estimate the oxygen fugacity at formation of the Inti CAI. Crystallization experiments by Grossman et al. (2008) on liquids of compositions similar to compact Type A, Type B1 and Type B2 CAIs showed that if such melts crystallized at 1509 K (the experimentally calibrated temperature), then the oxygen fugacity could be calculated from the Ti^{3+}/Ti^{4+} ratio in the Ti-rich pyroxene (fassaite). In addition to an assumed crystallization temperature of 1509K, the calculations assume equilibrium between fassaite, melilite and spinel. While Inti may not satisfy all of these prerequisites, the calculation of an estimated $\log f_{O_2}$ based on the Ti^{3+}/Ti^{4+} ratio in Inti fassaitic pyroxene provides a "litmus test" to compare the formation conditions of the CAI from comet 81P/Wild 2 with CAIs from the Allende meteorite.

A pair of equilibrium reactions involving Ti-rich pyroxene (Beckett and Grossman, 1986) can be used for estimating the oxygen fugacity of the formation environment of the comet 81P/Wild 2 refractory minerals:

$$4CaTi^{4+}Al_2O_6(T4P) + 4CaMgSi_2O_6(Di) \Leftrightarrow 4CaTi^{3+}AlSiO_6(T3P) + 2Ca_2MgSi_2O_7\ (Åk) + 2MgAl_2O_4\ (Sp) + O_2 \quad (1)$$

$$2CaAl_2SiO_6(CaTs) + 2CaMgSi_2O_6(Di) + 4CaTi^{4+}Al_2O_6(T4P) \Leftrightarrow 4CaTi^{3+}AlSiO_6(T3P) + 2Ca_2Al_2SiO_7\ (Ge) + 2MgAl_2O_4\ (Sp) + O_2 \quad (2)$$

where CaTs, Di, T3P and T4P represent the four endmember components of fassaite. T3P and T4P refer to endmember Ti-pyroxene with 3+ and 4+ oxidation states of Ti, respectively. Assuming that fassaite and melilite in Inti crystallized at 1509K, the temperature at which the above reactions were experimentally calibrated, the oxygen fugacity can be determined from the equilibrium constants for Equation (1) and Equation (2) above following the method of Grossman et al. (2008):

$$f_{O_2} = \frac{K'}{X_{Åk}^2} \cdot \frac{(X_{T4P} X_{Di} \gamma_{Di})^4}{(X_{T3P})^4} \quad (3)$$

$$f_{O_2} = \frac{K''}{(1 - X_{Åk})^2} \cdot \frac{(X_{CaTs} \gamma_{CaTs})^2 \cdot (X_{Di} \gamma_{Di})^2}{(X_{T3P} / X_{T4P})^4} \quad (4)$$

where X_i and γ_i are the mole fractions and activity coefficients, respectively, of each component. K' and K'' are constants equal to 1.321E-18 and 1.068E-17, determined by laboratory experiments at 1509K (Grossman et al., 2008). The average Inti melilite composition from measurements reported in Simon et al. (2008) is $X_{Åk} = 0.07$, nearly pure end-member gehlenite. Mole fractions reported in Table 1 for the components of fassaite in Equations (3) and (4) were determined from TEM-EDX quantification by assigning all Mg to diopside (Di), all Ti^{4+} to Ti^{4+}-bearing pyroxene (T4P), all Ti^{3+} to Ti^{3+}-bearing pyroxene (T3P) and the remainder to Ca-Tschermak's molecule (CaTs) based on the method reported by Beckett and Grossman (1986). The mole fraction ratio of 2:1 for T3P/T4P was determined from our EELS results above. These mole

fractions can be used to determine γ_{CaTs} and γ_{Di} following the method of Grossman et al. (2008) and, subsequently, the oxygen fugacity. The average $\log f_{O_2}$ values calculated by Equations (3) and (4) are reported Table 1.

This calculation results in an estimated oxygen fugacity of $\log f_{O_2}$ = -19.4±1.3, for the formation of Inti Ti-rich pyroxene (fassaite), where the uncertainty incorporates the uncertainty in the Ti^{3+}/Ti^{4+} ratio from EELS and uncertainties in the mole fractions of the minerals involved. This calculated oxygen fugacity should be considered a rough estimate, a basis for comparing the Inti formation conditions with those derived from other meteoritic fassaites: We have no evidence that the relevant mineral components in Inti crystallized at ~1500K nor that they were equilibrated, and the dependence of *K*' on temperature is unknown at present (Grossman et al., 2008).

4.3 Formation environments of Inti Ti-bearing components

Ti-bearing pyroxene (fassaite) in Inti has a Ti^{3+}/Ti^{4+} ratio of 2.0±0.2 ($Ti^{3+}/(Ti^{3+}+Ti^{4+})$ between 0.64 and 0.69), in agreement with Allende CAIs (Simon and Grossman, 2006) and other meteoritic fassaite (Dyl et al. 2005). Our calculated estimate of the oxygen fugacity at the formation of Inti Ti-pyroxene, $\log f_{O_2}$ = -19.4±1.3, is in excellent agreement with that reported for fassaite in Allende CAIs, $\log f_{O_2}$ = -19.8±0.9, and near the solar value of -18.1±0.3 (Grossman et al., 2008). These oxygen fugacities are given in Table 2 with values calculated from a Leoville CAI as well. The similarities can be seen graphically in Figure 5 by placing the oxygen fugacity value on a plot of $\log f_{O_2}$ versus temperature. Our derived oxygen fugacity value, combined with the typical solar system CAI mineralogy and ^{16}O-rich

isotopic composition of Inti (McKeegan et al., 2006; Simon et al., 2008; Zolensky et al., 2006), suggest that Inti most likely formed in the solar nebula, as opposed to an environment around another young star, a possibility that has been suggested as a means of explaining the presence of a CAI in a comet.

Although Inti fassaitic pyroxene shows a range of Ti contents, differing by more than a factor of 3 between lowest and highest TiO_2 content (see Table 1), it is interesting to note that the Ti EELS spectra for the approximately 50 EELS spectra collected are all remarkably similar. In fact, the Ti-L edge EELS from Inti fassaite are more uniform than those from the (much larger) Ti-pyroxene in the (much larger) Allende TS65 Type B2 CAI (Fig. 4a). This indicates that all of the Inti fassaite measured displays the same Ti^{3+}/Ti^{4+} ratio and likely formed in conditions of uniform oxygen fugacity. The variability in total Ti may reflect changing amounts of Ti available for incorporation into pyroxene. Both the variable Ti content in Ti-pyroxene and the variable V content in osbornite indicate that Inti cannot be considered fully equilibrated, despite its uniform Ti^{3+}/Ti^{4+} ratio.

In Inti osbornite, EELS indicates that some O may be present in some of the nitride grains, and no C was detected. Regardless of whether the osbornite contains O or C in solid solution, the presence of Ti(V)N alone requires that at least some of the refractory minerals in the Stardust CAI formed in a hot and highly reducing atmosphere with a high C/O ratio, ~0.8 to 1 (Ebel, 2006). The high C/O ratio suggests that the osbornite grains formed in a region very close to the proto-sun, since high C/O ratios (>0.79) are believed to have been present at heliocentric distances <0.5AU (Fukui and Kuramoto, 2005). The variable V content in osbornite grains only tens of nanometers in diameter also indicates possible dynamic conditions of formation for individual grains. (See Section 4.1.) Inti fassaitic pyroxene, on the other hand, has a

Ti^{3+}/Ti^{4+} ratio of ~2:1, in agreement with other solar system CAIs, indicating that the Inti fassaitic pyroxene formed in similar conditions to other CAIs from meteorites originating in the asteroid belt at heliocentric distances of several AU. We emphasize that the osbornite grains and other refractory minerals, including fassaitic pyroxene, may not have formed at the same time and in the same location, just as the osbornite and cometary ices certainly did not form simultaneously in the same location.

4.4 Transport of Inti components

Comet 81P/Wild 2 contains considerable ice, inconsistent with accretion in the inner solar system, and our Ti valence analysis on Inti fassaitic pyroxene is consistent with its formation in our own, rather than another, solar system. The current consensus among researchers is that comets formed in the outer solar system beyond 15 AU and that the osbornite and other refractory minerals were transported from the inner solar system outward over large distances (Brownlee et al., 2006). Several models have been proposed that predict relatively large-distance radial transport of solids in the early solar system, and we now have solid samples with which to test these models.

The X-wind model is frequently considered for material transport in the early solar system (Shu et al., 2001). This model predicts CAI formation as small, primitive particles that were repeatedly melted or partially melted, aggregated, partially vaporized and condensed in the solar nebula disk reconnection region, where the inner edge of the disk is truncated by the solar magnetosphere. In this model, the CAIs were ejected in the violent and energetic X-wind and redistributed in the accretion disk. A major difficulty with this model was pointed out by Desch and

Connolly (2007): The formation environment for the reconnection region is estimated to be 6 orders of magnitude more oxidizing than a solar composition gas, whereas meteoritic CAIs are generally consistent with formation in a gas of solar composition. Our measured Ti^{3+}/Ti^{4+} ratios in Inti fassaite confirm that the fassaite in the Stardust CAI, like other solar system CAIs, is consistent with a solar composition gas rather than a highly oxidizing gas. Finally, the presence of osbornite requires a formation environment significantly more reducing than a solar gas, one with a much higher C/O ratio. Thus, neither the Ti-bearing pyroxene (fassaite) nor the osbornite components in Inti are consistent with an X-wind formation scenario.

An alternative type of model considers transport of solids by mixing within the accretion disk. These models have grown more sophisticated over the years and consider a variety of effects including diffusion, gas drag and (turbulent) viscous flow (Bockelee-Morvan et al., 2002; Estrada et al., 2003) as well as settling due to gravity (Ciesla, 2007) and incorporate both radial and height dimensions. Such radial mixing models can transport crystalline silicates from the inner to outer disk regions relatively efficiently. Ciesla (2007) predicts that the 0.1 to 1.0 cm diameter CAIs found in meteorites could have been transported outward around the disk midplane while also being preserved in the solar nebula for the millions of years inferred between their formation and incorporation in meteorite parent bodies. Recent suggestions that the photophoretic force be added to such modelling (Mousis et al., 2007; Haack and Wurm, 2007) indicate that this additional outward force would generate a concentration of dust at the inner edge of the dust disk for localized rapid accretion and also solve the problem of over-homogenizing the disk. Radial mixing models have several advantages: In addition to allowing gradual condensation of volatiles on grain surfaces during transport, radial mixing models permit materials

formed very near the protosun to be transported and mixed with materials formed at greater heliocentric distances. Thus, the Inti osbornite, which formed in a highly-reducing environment very near the protosun (Fukui and Kuramoto, 2005), could have been incorporated into the Inti CAI with the Inti fassaitic pyroxene, formed in gas compositions that were approximately solar, and the CAI could then have been transported to the comet-forming region where it was eventually incorporated into the comet 81P/Wild 2.

5. SUMMARY AND CONCLUSIONS

The return of an inner solar system calcium-aluminum-inclusion, or CAI, in the NASA Stardust mission sample captured from the coma of an outer solar system comet, 81P/Wild 2 has raised provocative questions about the physiochemical conditions in the solar nebula and the dynamics of radial mass transport in the solar nebula accretion disk. To better elucidate the conditions and dynamics, we characterized the Ti-bearing refractory minerals, pyroxene (fassaite) and osbornite, in the Stardust CAI, Inti, by the scanning transmission electron microscopy analytical techniques of imaging, nano-diffraction, energy dispersive x-ray spectroscopy (EDX) and electron energy loss spectroscopy (EELS).

EELS data on several Inti fassaitic pyroxene grains, on pre-characterized fassaitic pyroxene from an Allende CAI and on endmember oxidation state standards show that the Inti fassaitic pyroxene has a Ti^{3+}/Ti^{4+} ratio of 2.0±0.2 like Allende CAIs. If equilibrium can be assumed among fassaitic pyroxene, spinel, diopside and gehlenite and crystallization occurred at 1509K, then the oxygen fugacity during Inti formation can be estimated from the Ti^{3+}/Ti^{4+} ratio. The $\log f_{O_2}$ estimated in this manner is

-19.4±1.3 for Inti. This estimate is in excellent agreement with those reported for Allende CAIs under identical assumptions and near the solar gas value. These results, combined with the typical CAI mineralogy and isotopic compositions observed for Inti, are consistent with solar system formation, and it is unlikely that Inti formed outside the solar system. Like other solar system CAIs, Inti likely formed in an approximately solar composition gas at a few AU from the proto-sun.

Inti also contains V-bearing osbornite, Ti(V)N. Osbornite, most likely an early condensate, forms at higher temperatures and C/O ratios than fassaitic pyroxene, in the highly reducing conditions predicted to have existed in the inner solar nebula within 0.5 AU of the proto-sun. Inti osbornite is present as nanometer-scale inclusions in the host phases anorthite, diopside and spinel. Fassaitic pyroxene has not yet been identified as a host for osbornite. As inclusions, these osbornite grains must have formed prior to, or simultaneously with, their host phases. The petrographic associations of Inti osbornite are not completely consistent with either of the two meteoritic cases (Isheyevo and ALH85085) known to date. Evidence for Ti-carbide and –oxide in solid solution in the Inti osbornite was sought by EELS and imaging. TiC was not detected, and TiO may be present, somewhat limiting the range of C/O ratio suitable for Inti osbornite formation. However, variable V contents prevent a definitive determination of the presence of TiO in the osbornite inclusions in Inti.

Details of chemistry in both the Inti osbornite and fassaitic pyroxene indicate fine-scale variations in this cometary CAI. Osbornite inclusions display variable amounts of V distributed heterogeneously in individual inclusions only tens of nanometers in diameter. Fassaitic pyroxene displays variable total Ti contents by EDX but uniform Ti^{3+}/Ti^{4+} ratios by EELS. We conclude that this CAI is not well-equilibrated and that the osbornite inclusions were likely never annealed at

temperatures sufficient to generate chemical homogenization. These results imply relatively early and rapid transport of Inti from the inner solar system to the outer solar system. The observed variability in mineral chemistry suggests that comet 81P/Wild 2 represents both a spatial and time capsule to investigate the early solar system. Such insight is invaluable to our further understanding the formation of comets and other bodies in the solar system.

Consideration of our analytical results with proposed material transport models appears to rule out the X-wind model, which yields highly oxidizing conditions in a reconnection region in the solar nebular disk. These formation conditions are inconsistent with both of the Ti-bearing refractory minerals in the Stardust CAI, Inti. Osbornite is stable in reducing environments, and the estimated oxygen fugacity derived from Inti fassaitic pyroxene indicates it formed in an approximately solar composition gas. Radial mixing models, on the other hand, allow the accretion of components from different heliocentric distances and, thus, different formation environments. Such models are more consistent with the oxidation environments inferred for the Inti mineral assemblage. A scenario made possible by radial mixing models is formation of tiny osbornite grains, tens of nanometers in diameter, within 0.5 AU of the proto-sun, rapid transport outward to a few AU where they were incorporated in CAI host minerals as the Inti CAI formed with its fassaitic pyroxene component. The Inti CAI, approximately 15 micrometers in diameter, may then have been transported outward to the comet-forming region beyond 15 AU where it accreted into comet 81P/Wild 2 with other materials and ices.

Acknowledgements. The authors wish to thank the reviewers … This research was funded in part by NASA grants NNH04AB49I, NNH06AD67I and NNH07AF99I to J. P. Bradley and by NASA grant NNH07AG46I to H. A. Ishii. S. B. Simon was

supported by NASA Grant NNG00GG00G to L. Grossman. G. Matrajt was supported by NASA Grant NNM05AA19G to D. Brownlee. M. Chi was supported by a LLNL SEGRF Fellowship during the research and preparation of this manuscript. Portions of this work were performed under the auspices of the U.S. Department of Energy by Lawrence Livermore National Laboratory under Contract DE-AC52-07NA27344.

References

Allende P. C., Lambert D. L., and Asplund M. (2002) A reappraisal of the solar photospheric C/O ratio. *Astrophys. J. Lett.* **573,** L137-L140.

Anders E. and Grevesse N. (1989) Abundances of the elements: Meteoritic and solar. *Geochim. Cosmochim. Acta* **53**, 197-214.

Beckett J. R. (1986) The origin of calcium-, aluminium-rich inclusions from carbonaceous chondrites: An experimental study. Ph. D. thesis, University of Chicago. 373 pp.

Beckett J. R. and Grossman L. (1986) Oxygen fugacities in the solar nebula during crystallization of fassaite in Allende inclusions. *Lunar Planet. Sci. XVII.* Lunar Planet. Inst., League City, TX, pp. *36-37*.

Bockelee-Morvan D., Gautier D., Hersant F., Hure J. M. and Robert F. (2002) Turbulent radial mixing in the solar nebula as the source of crystalline silicates in comets. *Astronomy & Astrophysics* **384**, 1107-1118.

Brownlee D., Tsou P., Aleon J., Alexander C. M. O., Araki T., Bajt S., Baratta G. A., Bastien R., Bland P., Bleuet P., Borg J., Bradley J. P., Brearley A., Brenker F., Brennan S., Bridges J. C., Browning N. D., Brucato J. R., Bullock E., Burchell M. J., Busemann H., Butterworth A., Chaussidon M., Cheuvront A., Chi M. F., Cintala M. J., Clark B. C., Clemett S. J., Cody G., Colangeli L., Cooper G., Cordier P., Daghlian C., Dai Z. R., D'Hendecourt L., Djouadi Z., Dominguez G., Duxbury T., Dworkin J. P., Ebel D. S., Economou T. E., Fakra S., Fairey S. A. J., Fallon S., Ferrini G., Ferroir T., Fleckenstein H., Floss C., Flynn G., Franchi I. A., Fries M., Gainsforth Z., Gallien J. P., Genge M., Gilles M. K., Gillet P., Gilmour J., Glavin D. P., Gounelle M., Grady M. M., Graham G. A.,

Grant P. G., Green S. F., Grossemy F., Grossman L., Grossman J. N., Guan Y., Hagiya K., Harvey R., Heck P., Herzog G. F., Hoppe P., Horz F., Huth J., Hutcheon I. D., Ignatyev K., Ishii H., Ito M., Jacob D., Jacobsen C., Jacobsen S., Jones S., Joswiak D., Jurewicz A., Kearsley A. T., Keller L. P., Khodja H., Kilcoyne A. L. D., Kissel J., Krot A., Langenhorst F., Lanzirotti A., Le L., Leshin L. A., Leitner J., Lemelle L., Leroux H., Liu M. C., Luening K., Lyon I., MacPherson G., Marcus M. A., Marhas K., Marty B., Matrajt G., McKeegan K., Meibom A., Mennella V., Messenger K., Messenger S., Mikouchi T., Mostefaoui S., Nakamura T., Nakano T., Newville M., Nittler L. R., Ohnishi I., Ohsumi K., Okudaira K., Papanastassiou D. A., Palma R., Palumbo M. E., Pepin R. O., Perkins D., Perronnet M., Pianetta P., Rao W., Rietmeijer F. J. M., Robert F., Rost D., Rotuni A., Ryan R., Sandford S. A., Schwandt C. S., See T. H., Schlutter D., Scheffield-Parker J., Simionivici A., Simon S., Sitnitsky I., Snead C. J., Spencer M. K., Stadermann F. J., Steele A., Stephan T., Stroud R., Susini J., Sutton S. R., Suzuki Y., Taheri M., Taylor S., Teslich N., Tomeoka K., Tomioka N., Toppani A., Trigo-Rodríguez J. M., Troadec D., Tsuchiyama A., Tuzzolino A. J., Tyliszczak T., Uesugi K., Velbel M., Vellenga J., Vicenzi E., Vincze L., Warren J., Weber I., Weisberg M., Westphal A. J., Wirick S., Wooden D., Wopenka B., Wozmiakiewicz P., Wright I., Yabuta H., Yano H., Young E. D., Zare R. N., Zega T., Ziegler K., Zimmerman L., Zinner E. and Zolensky M. (2006) Comet 81P/Wild 2 under a microscope. *Science* **314**, 1711-1716.

Brydson R., Williams B. G., Engel W., Sauer H., Zeitler E. and Thomas J. M. (1987) Electron energy-loss spectroscopy (EELS) and the electronic-structure of titanium-dioxide. *Solid State Communications* **64**, 609-612.

Ciesla F. J. (2007) Dust coagulation and settling in layered protoplanetary disks. *Astrophysical Journal* **654**, L159-L162.

Colliex C., Manoubi T. and Ortiz C. (1991) Electron-energy-loss-spectroscopy near-edge fine-structures in the iron-oxygen system. *Physical Review B* **44**, 11402-11411.

Desch S. J. and Connolly H. C. (2007) Inti did not form in an X-wind (and neither did most CAIs). *70th Meteoritical Society Meeting*, Tucson, AZ, #5073 (abstr.).

Dyl K. A., Simon J. I., Russell S. S. and Young E. D. (2005) Rapidly changing oxygen fugacity in the early solar nebula recorded by CAI rims. *Lunar Planet. Sci. XXXVI.* Lunar Planet. Inst., League City, TX. #1531 (abstr.).

Ebel D. (2006) Condensation of rocky material in astrophysical environments. In *Meteorites and Early Solar System II* (eds. D. S. Lauretta and H. Y. McSween). Univ. of Arizona Press, Tucson, AZ, pp. 253-277.

Egerton R. F. (1996) *Electron energy-loss spectroscopy in the electron microscope*. Plenum Press, New York.

Enomoto M. (1996) The N-Ti-V system (nitrogen-titanium-vanadium). *Journal of Phase Equilibria* **17**, 248-252.

Estrada P. R., Cuzzi J. N. and Showalter M. R. (2003) Voyager color photometry of Saturn's main rings: a correction. *Icarus* **166**, 212-222.

Fukui T. and Kuramoto, K. (2005) Evolution of oxygen isotopic composition and C/O ratio at late stage of protoplanetary accretion disk. Workshop on Oxygen in the Earliest Solar System, September 19-21, 2005. Gatlinburg, Tennessee, LPI Contribution No. 1278., p.18.

Galesic I., Angelkort C., Lewalter H., Berendes A. and Kolbesen B. O. (2000) Formation of transition metal nitrides by rapid thermal processing (RTP). *Physica Status Solidi a-Applied Research* **177**, 15-26.

Garvie L. A. J., Zega T. J., Rez P. and Buseck P. R. (2004) Nanometer-scale measurements of Fe3+/Sigma Fe by electron energy-loss spectroscopy: A cautionary note. *American Mineralogist* **89**, 1610-1616.

Grossman L., Beckett J. R., Fedkin A. V., Simon S. B. and Ciesla F. J. (2008) Redox conditions in the solar nebula: Observational, experimental and theoretical constraints. *Reviews in Mineralogy and Geochemistry* **68**, 93-140.

Haack H. and Wurm G. (2007) Life on the edge - Formation of CAIs and chondrules at the inner edge of the dust disk. *Meteoritics & Planetary Science* **42**, A62-A62.

Hutchison R., Williams I. P. and Russell S. S. (2001) Theories of planetary formation: constraints from the study of meteorites. *Philosophical Transactions of the Royal Society of London Series A - Mathematical Physical and Engineering Sciences* **359**, 2077-2091.

Ishii H. A., Krot A. N., Keil K., Nagashima K., Bradley J. P., Teslich N., Jacobsen B. and Yin Q. Z. (2008) Discovery of wadalite in Allende Type B CAI. *Lunar Planet. Sci. XXXIX.* Lunar Planet. Inst., League City, TX. #1989 (abstr.).

Joswiak D. J., Brownlee D. E. and Matrajt G. (2008) Surprisingly high abundance of Na and Cr-rich calcic pyroxenes in Stardust tracks. *Lunar Planet. Sci. XXXIX.* Lunar Planet. Inst., League City, TX. #2177 (abstr.).

Lazar P., Redinger J., Strobl J., Podloucky R., Rashkova B., Dehm G., Kothleitner G., Sturm S., Kutschej K., Mitterer C. and Scheu C. (2008) N-K electron energy-

loss near-edge structures for TiN/VN layers: an ab initio and experimental study. *Analytical and Bioanalytical Chemistry* **390**, 1447-1453.

Leapman R. D., Grunes L. A. and Fejes P. L. (1982) Study of the L23 edges in the 3d transition-metals and their oxides by electron-energy-loss spectroscopy with comparisons to theory. *Physical Review B* **26**, 614-635.

McKeegan K. D., Aleon J., Bradley J., Brownlee D., Busemann H., Butterworth A., Chaussidon M., Fallon S., Floss C., Gilmour J., Gounelle M., Graham G., Guan Y. B., Heck P. R., Hoppe P., Hutcheon I. D., Huth J., Ishii H., Ito M., Jacobsen S. B., Kearsley A., Leshin L. A., Liu M. C., Lyon I., Marhas K., Marty B., Matrajt G., Meibom A., Messenger S., Mostefaoui S., Mukhopadhyay S., Nakamura-Messenger K., Nittler L., Palma R., Pepin R. O., Papanastassiou D. A., Robert F., Schlutter D., Snead C. J., Stadermann F. J., Stroud R., Tsou P., Westphal A., Young E. D., Ziegler K., Zimmermann L. and Zinner E. (2006) Isotopic compositions of cometary matter returned by Stardust. *Science* **314**, 1724-1728.

Meibom A., Krot A. N., Robert F., Mostefaoui S., Russell S. S., Petaev M. I. and Gounelle M. (2007) Nitrogen and carbon isotopic composition of the Sun inferred from a high-temperature solar nebular condensate. *Astrophys. J.* **656**, L33-L36.

Mousis O., Petit J. M., Wurm G., Krauss O., Alibert Y. and Horner J. (2007) Photophoresis as a source of hot minerals in comets. *Astronomy & Astrophysics* **466**, L9-L12.

Papike J. J., Karner J. M. and Shearer C. K. (2005) Comparative planetary mineralogy: Valence state partitioning of Cr, Fe, Ti, and V among

crystallographic sites in olivine, pyroxene, and spinel from planetary basalts. *American Mineralogist* **90**, 277-290.

Petaev M. I., Meibom A., Krot A. N., Wood J. A. and Keil K. (2001) The condensation origin of zoned metal grains in Queen Alexandra Range 94411: Implications for the formation of the Bencubbin-like chondrites. *Meteoritics & Planetary Science* **36**, 93-106.

Simon S. B. and Grossman L. (2006) A comparative study of melilite and fassaite in Types B1 and B2 refractory inclusions. *Geochim. Cosmochim. Acta* **70**, 780-798.

Simon S. B., Joswiak D. J., Ishii H. A., Bradley J. P., Chi M. F., Grossman L., Aléon L., Brownlee D. E., Fallon S., Hutcheon I. D., Matrajt G. and McKeegan K. D. (2008) A refractory inclusion returned by Stardust from Comet 81P/Wild 2. *Meteoritics & Planetary Science*, in press.

Sparrow T. G., Williams B. G., Rao C. N. R. and Thomas J. M. (1984) L3/L2 White-line intensity ratios in the electron energy-loss spectra of 3d transition-metal oxides. *Chemical Physics Letters* **108**, 547-550.

Stolper E., Paque J. and Rossman G. R. (1982) The influence of oxygen fugacity and cooling rate on the crystallization of Ca-Al inclusions from Allende. *Lunar Planet. Sci. XIII.* Lunar Planet. Inst., League City, TX. pp. 772-773.

Weisberg M. K., Nehru C. E. and Prinz, M. (1988) Petrology of ALH85085: a chondrite with unique characteristics. *Earth Planet. Sci. Lett.* **91**, 19-32.

Zega T. J., Garvie L. A. J. and Buseck P. R. (2003) Nanometer-scale measurements of iron oxidation states of cronstedtite from primitive meteorites. *American Mineralogist* **88**, 1169-1172.

Zolensky M. E., Zega T. J., Yano H., Wirick S., Westphal A. J., Weisberg M. K., Weber I., Warren J. L., Velbel M. A., Tsuchiyama A., Tsou P., Toppani A., Tomioka N., Tomeoka K., Teslich N., Taheri M., Susini J., Stroud R., Stephan T., Stadermann F. J., Snead C. J., Simon S. B., Simionovici A., See T. H., Robert F., Rietmeijer F. J. M., Rao W., Perronnet M. C., Papanastassiou D. A., Okudaira K., Ohsumi K., Ohnishi I., Nakamura-Messenger K., Nakamura T., Mostefaoui S., Mikouchi T., Meibom A., Matrajt G., Marcus M. A., Leroux H., Lemelle L., Le L., Lanzirotti A., Langenhorst F., Krot A. N., Keller L. P., Kearsley A. T., Joswiak D., Jacob D., Ishii H., Harvey R., Hagiya K., Grossman L., Grossman J. N., Graham G. A., Gounelle M., Gillet P., Genge M. J., Flynn G., Ferroir T., Fallon S., Ebel D. S., Dai Z. R., Cordier P., Clark B., Chi M. F., Butterworth A. L., Brownlee D. E., Bridges J. C., Brennan S., Brearley A., Bradley J. P., Bleuet P., Bland P. A. and Bastien R. (2006) Mineralogy and petrology of comet 81P/Wild 2 nucleus samples. *Science* **314**, 1735-1739.

Figures and Figure Captions

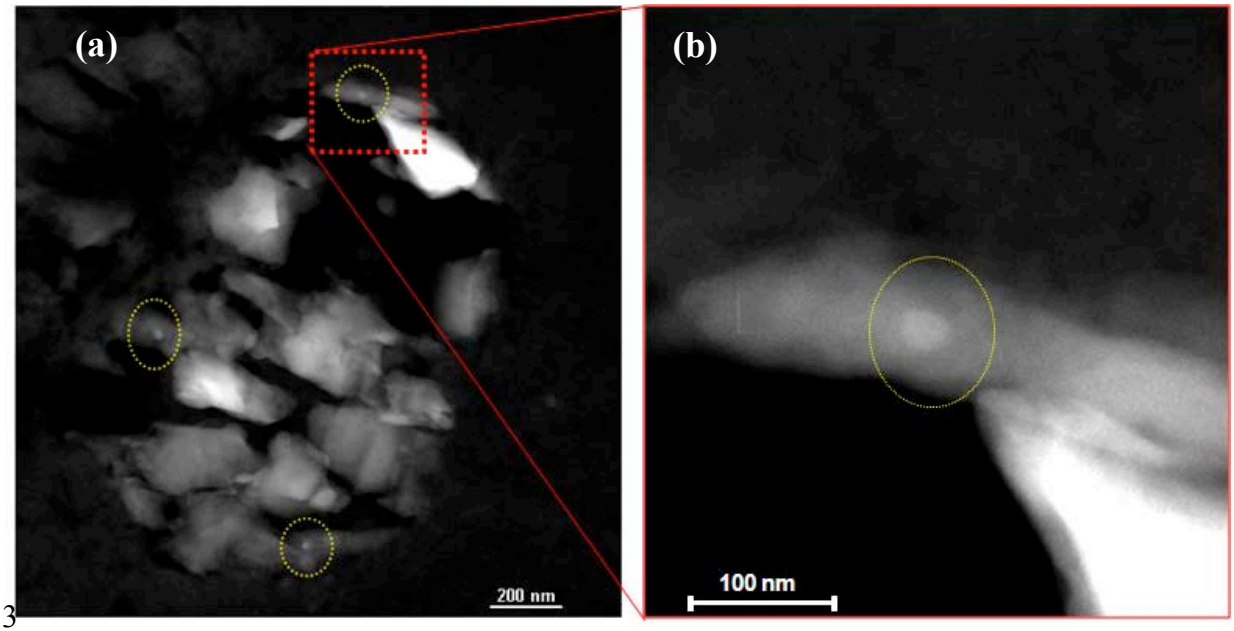

Figure 1. Scanning transmission electron microscopy dark field images showing (a) osbornite inclusions (circled) in a typical Inti ultramicrotomed sample from comet 81P/Wild 2 and (b) a magnified region containing one of the osbornite inclusions.

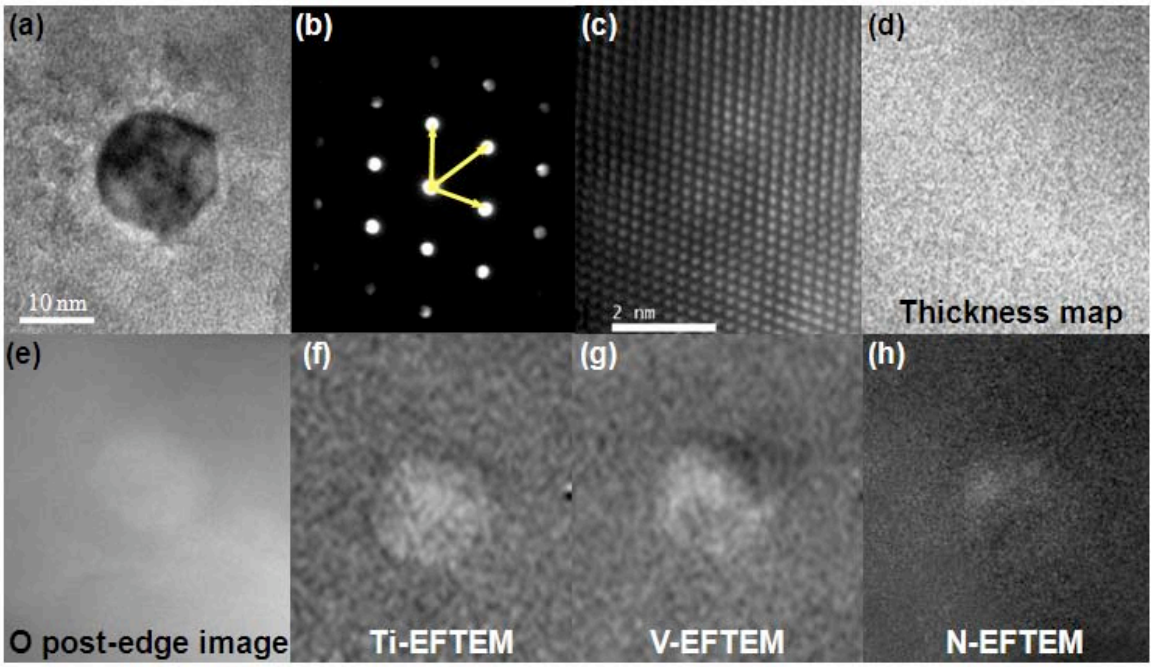

Figure 2. Images of a typical osbornite inclusion in its host matrix, the refractory mineral diopside. (a) TEM bright field image of this inclusion; (b) [011] zone axis diffraction pattern and (c) corresponding high resolution image of this inclusion; (d) thickness map of the area containing this inclusion; (e) O post-edge image of the same area in (d); (f)-(h) EFTEM images of Ti, V, and N, respectively.

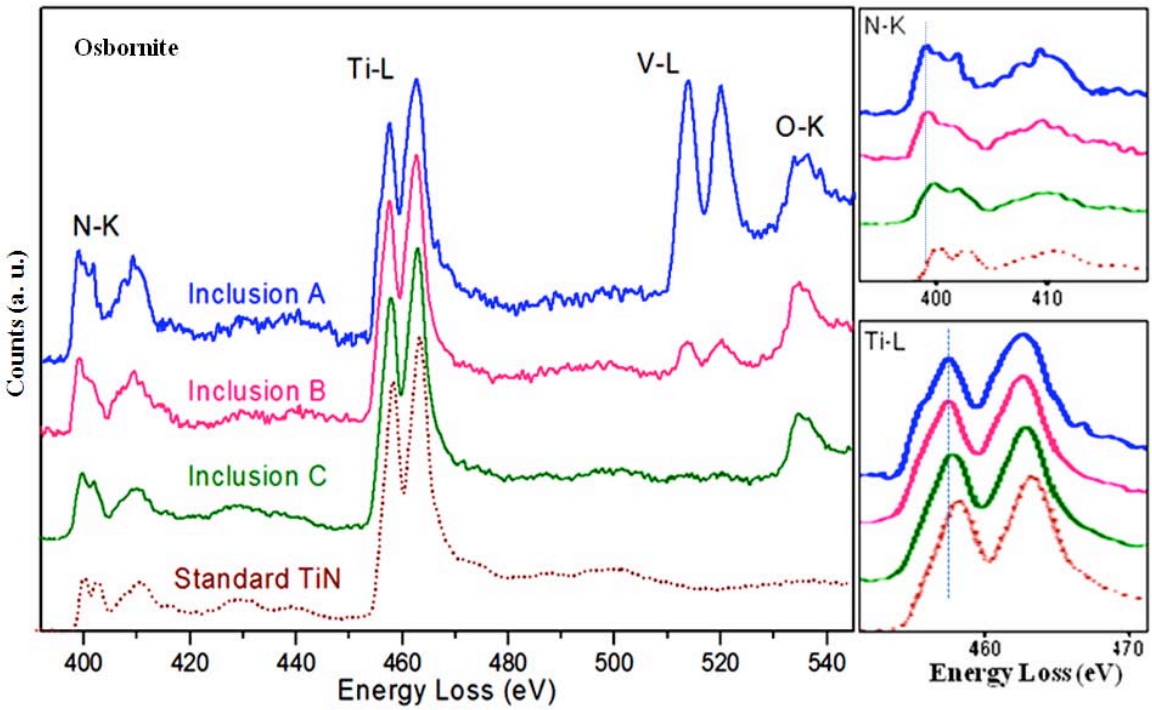

Figure 3. EEL spectra from osbornite inclusions in "Inti" show the existence of TiN and the variation of V content in these inclusions. Comparison of the spectrum of inclusion "C" and that from a standard TiN sample reveals the slight shift of the Ti-L edges to lower energies and the fine structure change of N-K edges in the spectrum of inclusion "C" (see the N-K and Ti-K edges magnified on the right hand side). The changes in edges energies and fine structures indicate changes of oxidation states.

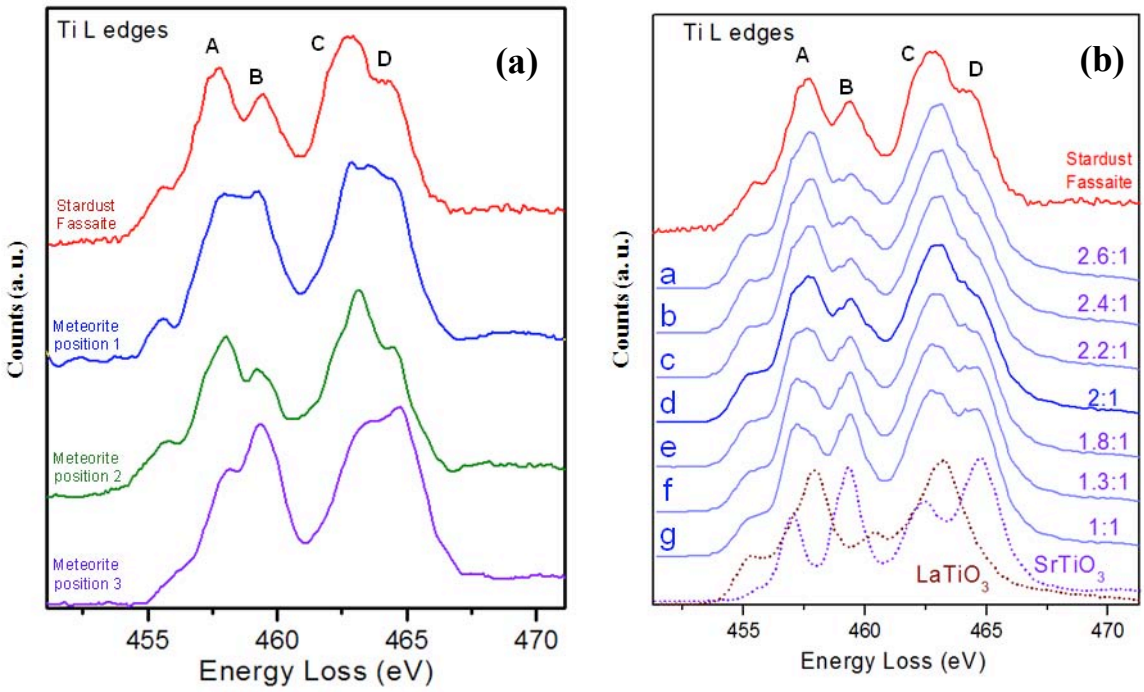

Figure 4. a) Ti-L edges of Stardust Ti-pyroxene compared with those from Ti-pyroxene from a CAI from the Allende meteorite, and (b) the Ti-L edges of Stardust Ti-pyroxene (top) and a series of spectra calculated from different ratios of the spectra from synthetic Ti^{3+} ($LaTiO_3$) relative to Ti^{4+} ($SrTiO_3$) end-members (bottom).

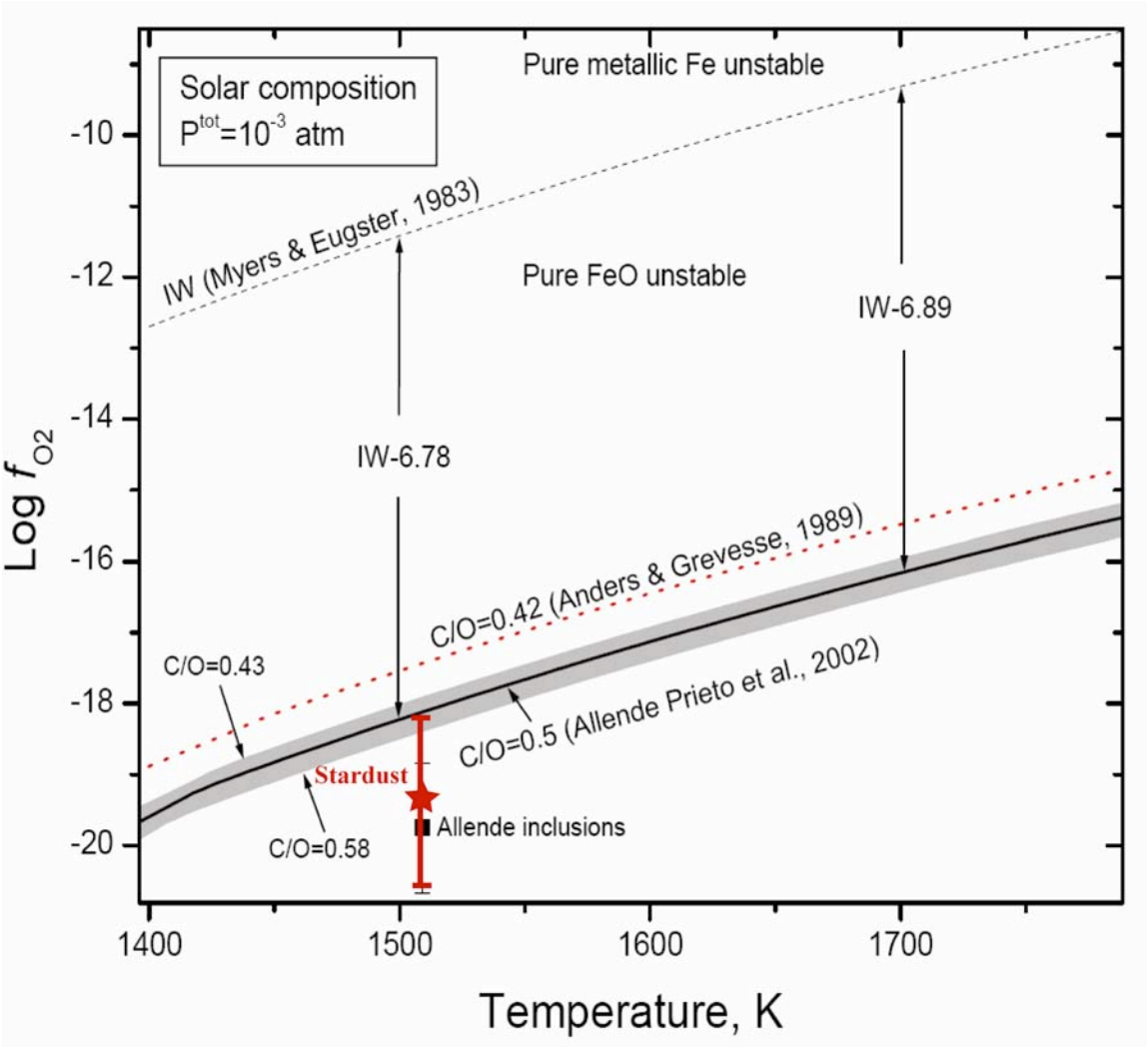

Fig. 5. Plot of log fO_2 vs. temperature for a system of solar composition at 10^{-3} atm for two estimates of the solar C/O ratio: 0.42 (Anders and Grevesse, 1989), and the preferred value, 0.5 (Allende et al., 2002). The iron-wüstite buffer curve of Myers and Eugster (1983) is shown for reference. The result for the Stardust CAI Inti falls very close to the value obtained for Allende inclusions (Grossman et al., 2008). Figure after Grossman et al. (2008).

Tables

Table 1. Compositions of Ti-pyroxene in the Inti CAI from comet 81P/Wild 2 and resulting estimates for log(fO_2).

Sample	1	2	3	4	5	6	7	8	9	10	11
					Cations per six oxygen anions						
Si	1.109	1.565	1.215	1.256	1.736	1.260	1.175	1.014	1.436	1.193	1.492
Al(IV)	0.891	0.435	0.785	0.744	0.264	0.740	0.825	0.986	0.564	0.807	0.508
Al(VI)	0.369	0.455	0.270	0.452	0.201	0.305	0.129	0.288	0.302	0.268	0.424
Mg	0.374	0.427	0.350	0.333	0.743	0.378	0.411	0.421	0.489	0.386	0.534
Ti	0.280	0.145	0.355	0.252	0.101	0.313	0.407	0.382	0.230	0.348	0.112
Ca	0.957	0.817	0.926	0.856	0.885	0.909	0.995	0.877	0.880	0.921	0.860
total	3.981	3.845	3.902	3.894	3.931	3.905	3.941	3.968	3.901	3.922	3.930
					Weight % oxides (analyses normalized to 100 wt%)						
MgO	6.84	8.08	6.44	6.19	13.93	6.97	7.46	7.69	9.10	7.09	10.00
Al_2O_3	29.14	21.28	24.51	28.15	11.02	24.39	21.91	29.46	20.36	24.96	22.09
SiO_2	30.21	44.10	33.30	34.83	48.48	34.64	31.81	27.63	39.84	32.63	41.64
CaO	24.33	21.48	23.67	22.16	23.07	23.33	25.14	22.32	22.79	23.52	22.40
Ti_2O_3	6.09	3.26	7.76	5.58	2.25	6.86	8.79	8.29	5.08	7.59	2.49
TiO_2	3.39	1.81	4.31	3.10	1.25	3.81	4.88	4.61	2.82	4.22	1.38
total TiO_2	10.09	5.41	12.83	9.24	3.74	11.35	14.50	13.70	8.43	12.54	4.14
					Mole fractions of Ti-pyroxene components						
Di	0.391	0.523	0.379	0.388	0.840	0.416	0.413	0.479	0.556	0.419	0.621
CaTs	0.315	0.299	0.238	0.317	0.046	0.240	0.178	0.086	0.183	0.203	0.249
T3P	0.195	0.118	0.256	0.196	0.076	0.229	0.273	0.290	0.174	0.252	0.087
T4P	0.098	0.059	0.128	0.098	0.038	0.115	0.136	0.145	0.087	0.126	0.043
					Average of log(fo_2) for each sample obtained using equilibrium reaction (1) and (3)						
log(fO_2)	-19.52	-19.15	-19.63	-19.53	-19.23	-19.51	-19.60	-19.67	-19.22	-19.54	-18.98
average log(fO_2)						-19.4	+/-1.3				

Total TiO_2 is given in weight % calculated with all Ti in TiO_2.

Standard relative errors based on counting statistics are ~5% for oxide abundances >1 wt% and ~10% for oxide abundances <1 wt%. Since oxygen is subject to greater absorption than other elements in TEM-EDX measurements, cation percents were converted to oxides (normalized to 100 weight %) from which cations per six oxygen anions were calculated.

Table 2. Comparison of oxygen fugacity of Stardust Inti to those of meteorites reported by other researchers.

sample	Stardust	Solar Gas	Allende	Leoville CA3 (WL rim)	Leoville CA3 (CAI interior)
$\log(f_{O2})$	-19.4±1.3	-18.1±0.3	-19.8±0.9	-12.3±1.8	-18.4±1.3
References	this work	Grossman et. al. 2008	Grossman et. al. 2008	Dyl et. al. 2005	Dyl et. al. 2005